NJC

Accepted Manuscript

This is an *Accepted Manuscript*, which has been through the Royal Society of Chemistry peer review process and has been accepted for publication.

Accepted Manuscripts are published online shortly after acceptance, before technical editing, formatting and proof reading. Using this free service, authors can make their results available to the community, in citable form, before we publish the edited article. We will replace this *Accepted Manuscript* with the edited and formatted *Advance Article* as soon as it is available.

You can find more information about *Accepted Manuscripts* in the Information for Authors.

Please note that technical editing may introduce minor changes to the text and/or graphics, which may alter content. The journal's standard Terms & Conditions and the Ethical guidelines still apply. In no event shall the Royal Society of Chemistry be held responsible for any errors or omissions in this *Accepted Manuscript* or any consequences arising from the use of any information it contains.

ROYAL SOCIETY OF CHEMISTRY

www.rsc.org/njc

Hierarchically porous $Li_{1.2}Mn_{0.6}Ni_{0.2}O_2$ as a high capacity and high rate capability positive electrode material

Shanmughasundaram Duraisamy, Tirupathi Rao Penki and Munichandraiah Nookala[#]

Department of Inorganic and Physical Chemistry, Indian Institute of Science, Bangalore - 560012, India

Abstract

Layered composite samples of lithium excess manganese oxide ($Li_{1.2}Mn_{0.6}Ni_{0.2}O_2$) are prepared by reverse microemulsion route employing a soft polymer template and studied as a positive electrode material. The product samples possess dual porosity with distribution of pores at 3.5 and 60 nm. Pore volume and surface area decrease by increasing the temperature of preparation. Nevertheless, the electrochemical activity of the composite increases with an increase in temperature. The discharge capacity values of the samples prepared at 800 and 900 ^{o}C are about 240 mAh g^{-1} at a specific current of 25 mA g^{-1} with a good cycling stability. The composite sample heated at 900 ^{o}C possesses a high rate capability with discharge capacity of 100 mAh g^{-1} at a specific current of 500 mA g^{-1}. The high rate capability is attributed to porous nature of the composite sample.

Key words: Polymer template; porous materials; lithium excess manganese oxide composite; high discharge capacity; high rate capability.

[#]Author for correspondence, e-mail: muni@ipc.iisc.ernet.in

New Journal of Chemistry Accepted Manuscript

1. Introduction

Research activities on Li-ion batteries have increased in the recent past because of their attractive energy density.[1, 2] These batteries are successfully used for extended applications in small sizes at present and they are anticipated to be useful in large sizes for applications such as electric vehicles. Although the energy density of the present Li-ion batteries is the greatest among rechargeable batteries, future requirements such as electric vehicle applications need still increased energy density. The next generation Li-ion batteries, thus, need novel electrode materials which can provide greater discharge capacity than the present materials, in addition to the need that they should be safe, inexpensive, non-toxic and environmental friendly.

At present, $LiCoO_2$, $LiMn_2O_4$ and $LiFePO_4$ either in their pure states or with partial substitutions of the transition metals, are employed as the positive electrode materials in Li-ion batteries. The discharge capacity values of $LiCoO_2$, $LiMn_2O_4$ and $LiFePO_4$ are 140, 130 and 170 mAh g^{-1}, respectively.[3] Li-ion batteries with greater energy density than the present batteries need the positive electrode materials of greater discharge capacity. Li_2MnO_3 is considered similar to the layered $LiCoO_2$ and its formula can also be presented as $Li(Li_{0.33}Mn_{0.67})O_2$.[4] One third of the octahedral sites meant for Mn in the crystal lattice are occupied by Li atoms. On the basis of the total available Li in Li_2MnO_3, a discharge capacity of 456 mAh g^{-1} is expected, provided the compound is electrochemically active. However, Li_2MnO_3 is not electrochemically active because the oxidation state of Mn is +4 and it cannot be oxidized to +5 when Li is extracted from the structure. Nevertheless, several publications have appeared with different procedures for activation of Li_2MnO_3 and with varying capacity values.[5-14] The initial discharge capacity values are generally high for the activated phases of Li_2MnO_3, but cycling instability is observed in all reports. In order to enhance the cycling stability, composites of Li_2MnO_3 with other layered lithiated transition metal oxides such as

New Journal of Chemistry Accepted Manuscript

$LiCoO_2$ are studied.[15-19] Namata et al.,[15] substituted Co in $LiCoO_2$ by Mn and Li together (1 Co by 0.67 Mn + 0.33 Li) in a wide range of compositions. When cycled between 3.00 and 4.30 V, there was a decrease in discharge capacity with an increase in concentration of Mn and Li substituted for Co. Pure phase of $LiCoO_2$ provided the highest capacity among several compositions studied.[15] Composites of Li_2MnO_3 and $LiMn_{0.5}Ni_{0.5}O_2$ were studied by Thackeray group.[16] It was reported that the cations of the transition metal layers were not homogeneously distributed as a solid solution, but were distributed in an irregular manner in domains with short range order.[16] Electrochemical activity was induced in Li_2MnO_3 component of the composite by a loss of Li_2O. A composite of Li_2MnO_3 with a layered oxide consisting of Mn, Ni and Co were also studied by Thackeray group.[17] On cycling between 2.00 and 4.60 V, a stable capacity of about 180 mAh g^{-1} was obtained. Electrochemical characterization of Li_2MnO_3-$Li[Ni_{1/3}Co_{1/3}Mn_{1/3}]O_2$-$LiNiO_2$ composite was reported by Lim et al.[18] A discharge capacity of about 250 mAh g^{-1} at a specific current of 20 mA g^{-1} was obtained. Synthesis of $Li_2MnO_3.LiMn_{1/3}Ni_{1/3}Co_{1/3}O_2$ was carried out by self-combustion reaction by Aurbach group.[19] A discharge capacity of 220 mAh g^{-1} was reported.[19] A study of publications including the above references suggests that the electrochemically inactive Li_2MnO_3 phase could be converted into an active stable phase by structural integration with another electrochemically active layered phase.

In addition to the high discharge capacity, an electrode material needs to possess high rate capability for the purpose of fast charge or/and discharge. Porous materials are expected to possess high rate capability because the electrolyte can creep into particles and enhance the contact area of the electroactive surface with the electrolyte.[20] As a result, the material can withstand an enhanced specific current during charge-discharge cycling. Furthermore, the electrode material can tolerate volume expansion and contraction that may occur during charge-discharge processes. To the best of authors' knowledge, there are no reports on the

New Journal of Chemistry Accepted Manuscript

synthesis of porous composites of Li_2MnO_3. In the present study, $0.5Li_2MnO_3$: $0.5LiMn_{0.5}Ni_{0.5}O_2$ (composition: $Li_{1.2}Mn_{0.6}Ni_{0.2}O_2$) is prepared by inverse microemulsion route assisted by a soft polymer template, namely, Pluronic acid (F068). The composite samples prepared at different temperatures possess mesoporosity resulting in a high discharge capacity, a high rate capability and also good cycling stability.

2. Experimental

High purity chemicals, namely lithium nitrate (Aldrich), manganese nitrate tetrahydrate (Aldrich), nickel nitrate hexahydrate (SD Fine Chemicals), Pluronic acid [F068, poly$(EO)_{78}$-poly$(PO)_{30}$-poly$(EO)_{78}$, where EO and PO are ethyleneoxide and propyleneoxide units, respectively; molecular weight ~8400; Aldrich], lithium dodecylsulfate (LDS, Aldrich), cyclohexane (Merck), n-butanol (SD Fine Chemicals), H_2SO_4 (SD Fine Chemicals), lithium ribbon (0.75 mm thickness, Aldrich), acetylene black (AB, Alfa Aesar), poly(vinylidene fluoride) (PVDF, Aldrich), 1-methyl-2-pyrrolidinone (NMP, Aldrich) and 1M $LiPF_6$ dissolved in ethylene carbonate, diethyl carbonate and dimethyl carbonate (2:1:2 v/v) electrolyte (Chameleon) were used as received.

For the preparation of composite samples, reverse microemulsion route involving F068 as a soft template was employed. For the oil phase, F068 (1.0 g) was dissolved in a mixture of 51.2 ml cyclohexane and 6.2 ml n-butanol. Then 0.225 g LDS was added and stirred for 3 h to get a transparent liquid. 1.947 g lithium nitrate, 3.219 g manganese nitrate tetrahydrate and 1.244 g nickel nitrate hexahydrate were dissolved in 15 ml double-distilled water. About 10% excess of lithium nitrate than the stoichiometric quantity was dissolved. The aqueous phase was transferred to the oil phase and stirred for 12 h by a magnetic pellet at ambient temperature. The emulsion was slowly evaporated at 110 ^{o}C. A green colour gel was

New Journal of Chemistry Accepted Manuscript

obtained. Samples of the gel were heated in air at different temperatures between 500 and 900 ^{o}C for 12 h. Black coloured powder samples were obtained.

The powder XRD patterns were recorded by using Philips X-PertPro diffractometer (40 kV and 30 mA) using Cu K_{α} (λ = 1.5418 Å) as the radiation source. Nitrogen adsorption-desorption isotherms were recorded at -196 ^{o}C by using Micromeritics surface area analyzer model ASAP 2020. The specific surface area was calculated using Brunauer-Emmett-Teller (BET) method in the relative pressure (p/p_0) range 0.05-0.25 from the adsorption branches of the isotherms. The pore size distribution was calculated by Barrett-Joyner-Halenda (BJH) method from the desorption branches. The morphology was studied using a Gemini Technology scanning electron microscope (SEM) model ULTRA 55, and JEOL Co. transmission electron microscope (TEM) model JEOL- JEM 2100F. The thermogravimetric analysis (TGA) curves were recorded from ambient temperature to 900 ^{o}C at a heating rate of 10 ^{o}C min^{-1} under the flow of O_2 gas by using thermal analyzer NETZSCH model TG 209 FI. The chemical composition analysis of the composite sample was carried out by inductive coupled plasma atomic emission spectroscopy using Varion inductive coupled spectrometer model Vista-PRO

Electrodes were made by mixing the active material (80 wt%), AB (10 wt%) and PVDF (10 wt%) in a mortar. A few drops of NMP were added and mixed to obtain slurry. A stainless steel disk (16 mm diameter) was cleaned with soap and water, etched in 30% dilute HNO_3, rinsed with double-distilled water followed by acetone and air dried. The slurry was coated on a pre-treated stainless steel disk and dried at 110 ^{o}C under vacuum. The coating and drying steps were repeated to obtain the mass of active material in the range 3-5 mg cm^{-2}. Lithium metal foil was used as the counter electrode and a Celgard porous polypropylene membrane (2400) was used as the separator. A commercial electrolyte of 1M $LiPF_6$ dissolved in ethylene carbonate, diethyl carbonate and dimethyl carbonate (2:1:2 v/v) was used as the

New Journal of Chemistry Accepted Manuscript

electrolyte. Coin cells CR2032 (Hohsen Corporation, Japan) were assembled in an argon environment glove box MBraun model UNILAB. The cells were cycled in the voltage range from 2.00 to 4.80 V at different current densities at room temperature. Cyclic voltammetry and charge-discharge cycling experiments were carried out using Biologic potentiostat/galvanostat model VMP3. The rate capability was studies by using Bitrode battery cycling equipment. The galvanostatic intermittent titration technique (GITT) experiments were carried out by using electrochemical analyser, CHI608C (CH Instruments, Inc. USA) in an air-conditioned room at 22±1 ^{o}C

3. Results and discussion

3.1. Synthesis: Soft chemical synthesis by inverse microemulsion route is useful for the preparation of small particles. By dispersing a small volume of an aqueous phase consisting of the reactants in a large volume of an immiscible non-aqueous phase, the reactants are present in micrometer sized aqueous reaction zones and particles of the products are limited to the size of the surfactant stabilizer aqueous droplets. Sub-micrometer/nanometer size product particles are synthesized by this route.[21] The presence of polymeric templates such as F068 in the reaction medium facilitates the product particles to develop porosity. The presence of hydrophilic EO block and hydrophobic PO block is responsible for generating porosity on the product particles.[22] By combining the salient features of inverse microemulsion and polymeric templates, synthesis of porous, sub-micrometer size cathode materials, namely, $LiFePO_4$ and $LiNi_{1/3}Mn_{1/3}Co_{1/3}O_2$, were synthesized in our laboratory.[23-25] A similar procedure was adopted for preparation of $0.5Li_2MnO_3$:$0.5LiMn_{0.5}Ni_{0.5}O_2$ composite in the present work.

New Journal of Chemistry Accepted Manuscript

3.2. Thermogravimetric analysis: The gel obtained after evaporation of solvents at 110 ^{o}C was subjected to thermogravimetry (Fig. 1). There is a continuous loss of mass between the ambient and about 180 ^{o}C due to the removal of solvents and decomposition of nitrates. About 14% of weight loss is observed at 180 ^{o}C. There is about 7% of weight decrease between 180 and 280 ^{o}C, which is likely due to decomposition of the polymer template and small 3% weight loss between 280 and 416 ^{o}C is attributed to. The mass of the sample is fairly constant between 416 and 900 ^{o}C. Therefore, samples of the gel were heated at several temperatures from 500 to 900 ^{o}C for 12 h. The samples prepared at 500, 600, 700, 800 and 900 ^{o}C are hereafter referred to as S5, S6, S7, S8 and S9, respectively.

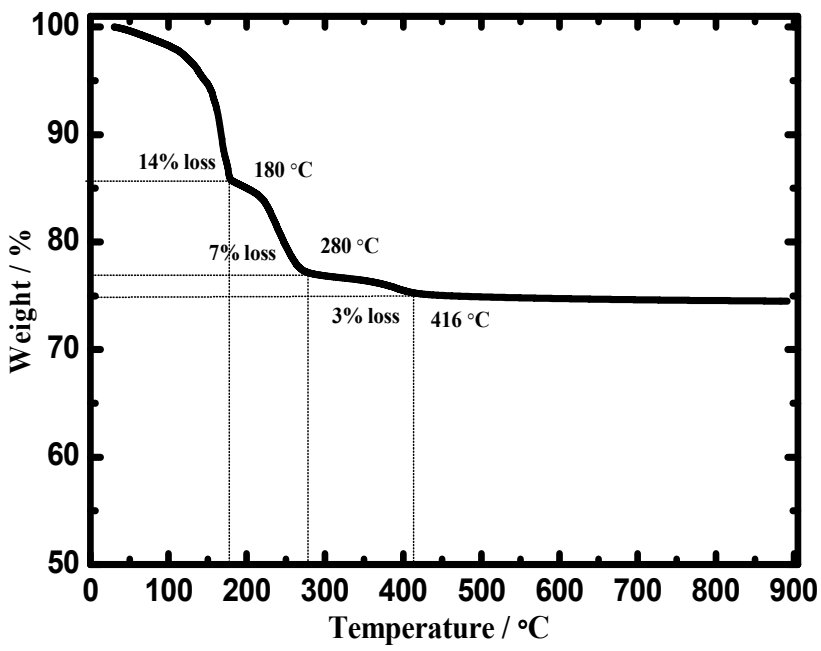

Fig. 1. Thermogravimetry of the precursor.

3.3. XRD studies: Powder XRD patterns of the samples prepared at different temperatures are shown in Fig. 2. All samples exhibit crystalline nature. The standard pattern of Li_2MnO_3 (JCPDS No. 84-1634) is shown as curve (i). The pair of peaks expected around 65° for a layered compound of α–$NaFeO_2$ structure is not well resolved (Fig. 2 curves (ii), (iii) and (iii)) for S5, S6 and S7 samples. Thus, the samples prepared at 500, 600 and 700 ^{o}C are not

New Journal of Chemistry Accepted Manuscript

well formed layered structures, although the presences of any impurity reflections are not observed.

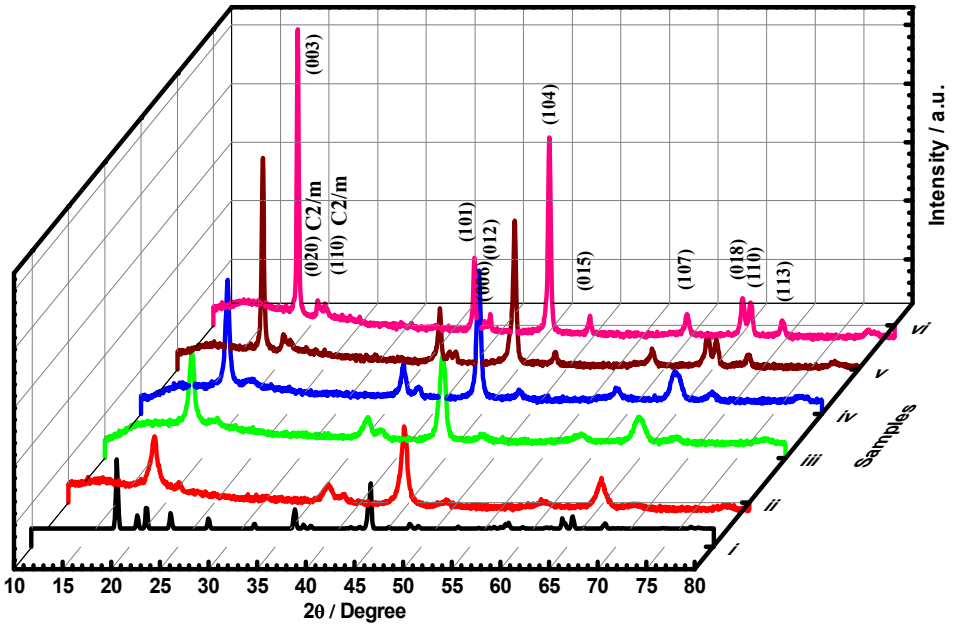

Fig. 2. Powder XRD patterns of standard pattern of Li_2MnO_3 (i), $0.5Li_2MnO_3$:$0.5LiMn_{0.5}Ni_{0.5}O_2$ samples S5 (ii), S6 (iii), S7 (iv), S8 (v) and S9 (vi).

Nevertheless, the XRD patterns of samples S8 and S9 indicate well grown layered crystalline structures (Fig. 2 curves (v) and (vi)). The structure of Li_2MnO_3 was determined by using single crystal X-ray diffraction by Strobel and Andron.[26] Li_2MnO_3 was described as $Li[Li_{1/3}Mn_{2/3}]O_2$ structure of O3-type where the octahedral sites of inter-slab are occupied by lithium ion and octahedral sites of the slab by lithium and manganese ions in 1:2 ratio. The XRD patterns (Fig. 2 curves (v) and (vi)) agree well with the standard pattern of the layered structure (JCPDS file No. 84-1634) (Fig. 2 curve (i)). The (020) and (110) reflections in 2θ range 20-23° indicate Li-Mn ordering in the mixed cation layer and these superstructure reflections are signatures for Li_2MnO_3. Lattice constants were calculated using FullProof Suite program (Table 1). The XRD patterns are indexed based on α–$NaFeO_2$ structure with

New Journal of Chemistry Accepted Manuscript

R3-m space group and the lattice parameters are listed in Table 1. It is known that the material has layered structure if the c/a ratio is greater than 4.9.[27, 28] It is seen (Table 1) that the c/a ratio is greater than 4.9 for the samples S8 and S9 indicating the layered structure characteristics. Furthermore, the intensity ratio of (003) and (104) peaks ($I_{(003)}/I_{(104)}$) is a sensitive parameter, which reflects the cation order between Li and transition metal layers. It is seen in Table 1 that the $I_{(003)}/I_{(104)}$ ratio is greater than unity, but it increases with an increase in temperature of preparation. Thus the sample S9 is superior to the rest of the samples. Therefore, this sample exhibits better electrochemical performance as expected. The average crystallite sizes of Li_2MnO_3 samples were calculated from (003) diffraction peaks using Scherrer equation [23] and they were in 100-200 nm range.

Table 1. Lattice parameters of the samples S7-S9.

Sample	a (nm)	c (nm)	c/a	$I_{(003)}/I_{(104)}$
S8	0.2859	1.4271	4.99	1.19
S9	0.2859	1.4270	4.99	1.25

3.4. Microscopy: SEM micrographs of $0.5Li_2MnO_3$:$0.5LiMn_{0.5}Ni_{0.5}O_2$ composite samples are presented in Fig. 3. The S5 sample consists of micrometers sized particles with flake-like morphology (Fig. 3A). On further increasing the temperature of preparation, the particle size increases gradually (Fig. 3B-E), as expected. Agglomerated particles of varied dimensions are present in S9 sample (Fig. 3E). TEM images (Fig. 4A-E) also support the information derived from SEM images (Fig. 3). The SAED pattern is shown in Fig. 4F. A diffused pattern is obtained for sample S9 indicating ploycrystallinity. The lattice fringes with interplanar spacing d = 4.74 Å are observed in the HRTEM image (Fig. 4G) of S9 sample, which corresponds to (003) plane of Li_2MnO_3.

New Journal of Chemistry Accepted Manuscript

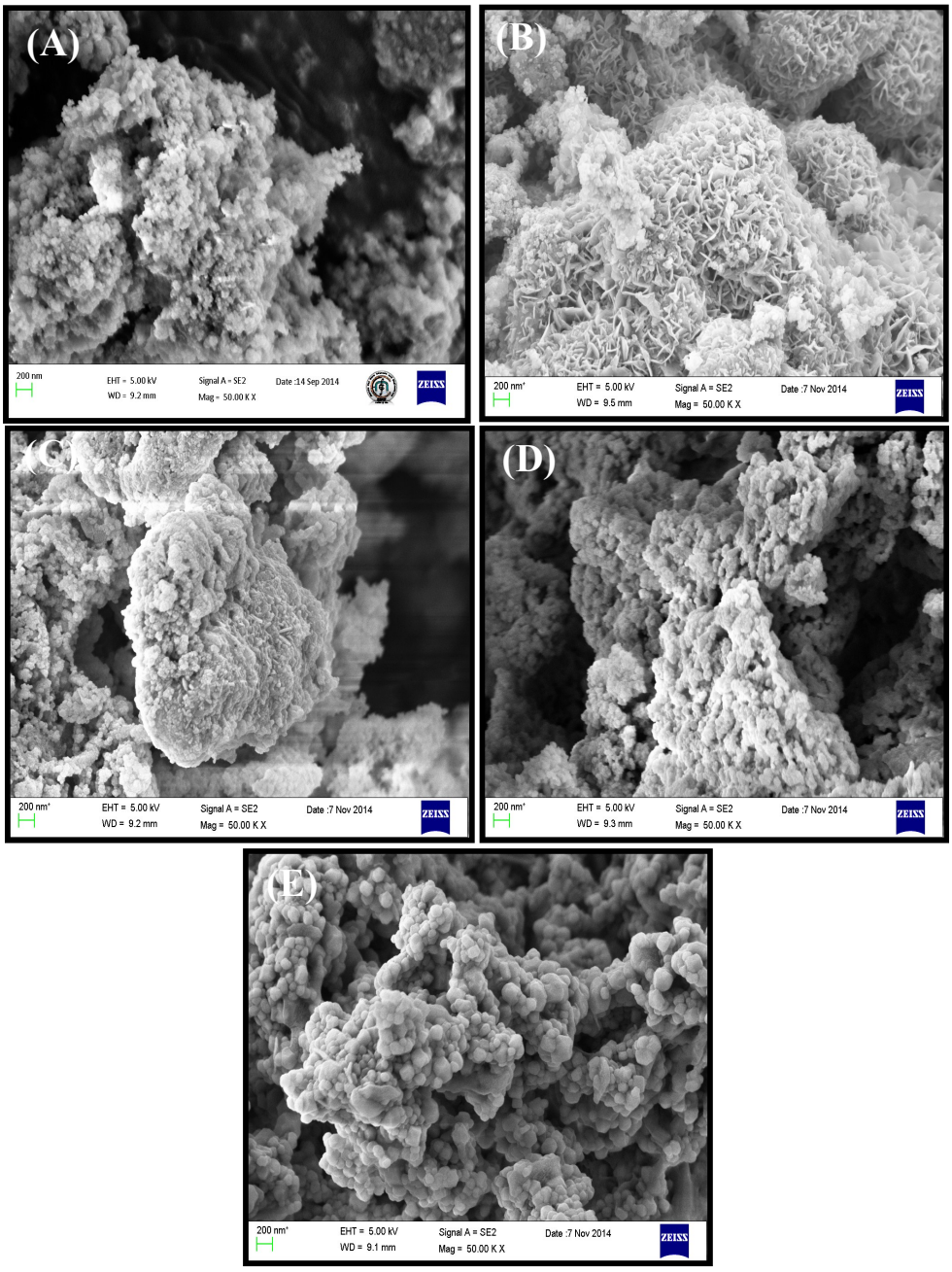

Fig. 3. SEM micrographs of (A) S5, (B) S6, (C) S7, (D) S8 and (E) S9 samples of $0.5Li_2MnO_3{:}0.5LiMn_{0.5}Ni_{0.5}O_2$.

New Journal of Chemistry Accepted Manuscript

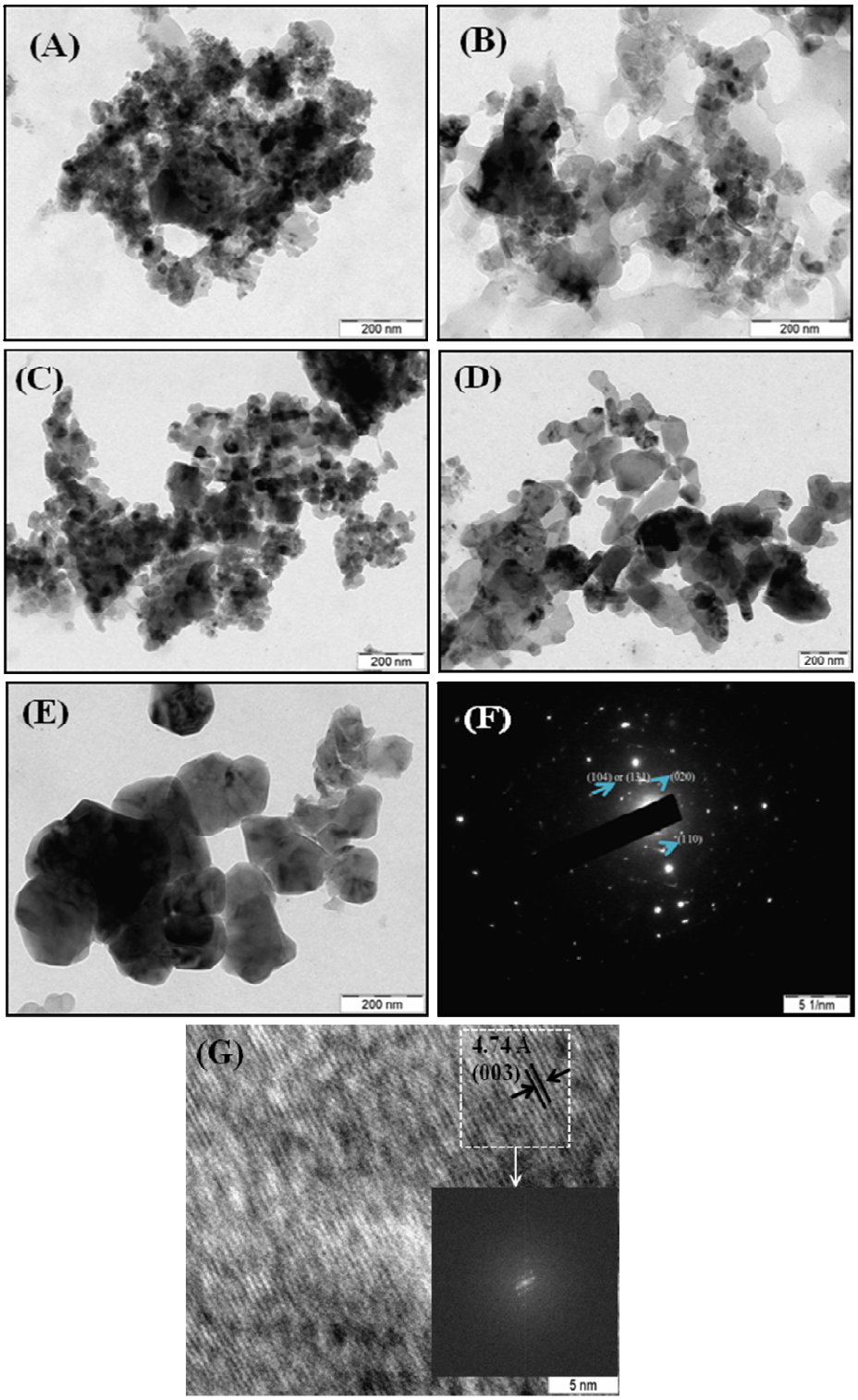

Fig. 4. TEM images of S5 (A), S6 (B), S7 (C), S8 (D) and S9 (E). Selective area electron diffraction (SAED) and high resolution transmission electron microscope (HRTEM) image of S9 sample of composite $0.5Li_2MnO_3$:$0.5LiMn_{0.5}Ni_{0.5}O_2$.

New Journal of Chemistry Accepted Manuscript

3.5. Surface area and porosity: Nitrogen adsorption/desorption isotherms and BJH porosity curves are presented in Fig. 5. The adsorption and desorption branches do not merge in the pressure region p/p_o between 0.50 and 0.99 for all samples suggesting the porous nature of the samples. The amount of N_2 adsorbed on S5 sample (Fig. 5A (i)) at $p/p_o = 0.99$ is about 54 $cm^3\ g^{-1}$, which is considered as high. The BET surface area obtained in p/p_o ratio 0.1 - 0.2 range of the adsorption isotherm is 17.5 $m^2\ g^{-1}$. The porous nature is clearly reflected in BJH curves (Fig. 5B). There is a narrow distribution of pores at 3.6 nm and another broad distribution of larger pores around 30 nm diameter for S5 sample (Fig. 5B (i)). The BET surface area, cumulative pore volume and pores diameter obtained for all samples are listed in Table 2. The BET area obtained for S6 sample is also 8.3 $m^2\ g^{-1}$, but pore volume decreases marginally (Table 2 and Fig. 5B (ii)). On further increasing the temperature of preparation, the sample S7 has decreased surface area (8.0 $m^2\ g^{-1}$) and also lower pore volume. However, the pore diameter remains at 3.5 nm and broad pores around 30 nm. The decreasing tendency of both surface area and pore volume continues by increasing the temperature of preparation. The BET area of sample S9 is 3.1 $m^2\ g^{-1}$. The BJH curves indicate the existence of porosity in all samples, although the pore volume decreases by increasing the temperature of preparation (Table 2 and Fig. 5B). Increase in particle size and also density on increasing the temperature of preparation could be the causes for a decrease in pore volume of the composite samples. Nevertheless, duel porosity is present on all samples, which is attributed to the presence of the polymeric template in the reaction medium of preparation. These kinds of hierarchically porous samples are beneficial for battery applications. The pores allow the electrolyte to creep inside the particles, thereby increasing the contact area. This leads to high rate capability of the electrode material. Furthermore, the particles can withstand expansion/contraction cycles that generally occur during charge/discharge cycles. This prevents pulverization of electrode particles and increases the cycling stability. Similar

New Journal of Chemistry Accepted Manuscript

to this data, hierarchically porous nature is reported for MnO_2[29], $LiMn_2O_4$[29, 30] and $LiFePO_4$[24] samples.

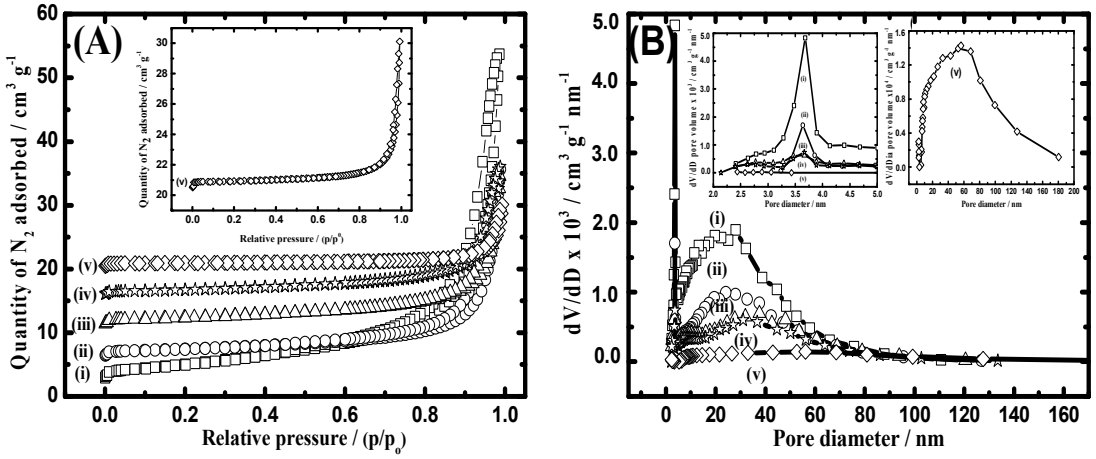

Fig.5. (A) N_2 adsorption/desorption isotherms and (B) pore size distribution (BJH) curves of $0.5Li_2MnO_3$:$0.5LiMn_{0.5}Ni_{0.5}O_2$ samples S5 (i), S6 (ii), S7 (iii), S8 (iv) and S9 (v) samples. The curve (v) is expanded and shown as inset in (B). In (A), curves (ii), (iii), (iv) and (v) are, respectively, vertically shifted by 5, 10, 15 and 20 units of Y-axis scale relative to the position of curve (i).

Table 2. BET surface area, cumulative pore volume and pore diameter of the samples S5-S9.

S.No	Sample	BET surface area (m^2/g)	Cumulative pore volume (cm^3/g)	Pore diameter (nm)
1	S5	17.5	0.082	3.6, 28
2	S6	8.3	0.046	3.6, 24
3	S7	8.0	0.036	3.5, 38
4	S8	5.9	0.032	3.7, 32
5	S9	3.1	0.014	2.9, 55

3.6. Cyclic voltammetry: Cyclic voltammograms of S7, S8 and S9 samples recorded in the potential range between 2.0 and 4.8 V with scan rate 0.1 mV s^{-1} for three repetitive cycles are presented in Fig. 6. For S7 sample (Fig. 6A), an oxidation current peak appears at 3.86 V in the first cycle when the cell was subjected to potential sweep from the open-circuit voltage (around 3.28 V). This current peak is followed by another large current peak at 4.69 V. In the

New Journal of Chemistry Accepted Manuscript

reverse sweep from 4.80 to 2.00, a small cathodic current peak appears at 3.67 V. Among the two transition metals present in $LiMn_{0.5}Ni_{0.5}O_2$ part of the composite, the oxidation state of Mn and Ni are +4 and +2, respectively.[31, 32] Accordingly, the low potential oxidation current peak at 3.68 V (Fig. 6A) is attributed to the extraction of Li^+ from $LiMn_{0.5}Ni_{0.5}O_2$ part of the composite resulting from the oxidation of Ni^{2+} to Ni^{4+}.[33] The oxidation current peak appearing at 4.69 V (Fig. 6A) is due to the activation of Li_2MnO_3 part present in the composite. The electrochemical activation of Li_2MnO_3 occurs due to the loss of O_2 from the surface of the particles.[34, 35]

$$Li_2MnO_3 \rightarrow MnO_2 + 2Li^+ + 0.5\,O_2 + 2e^- \quad (1)$$

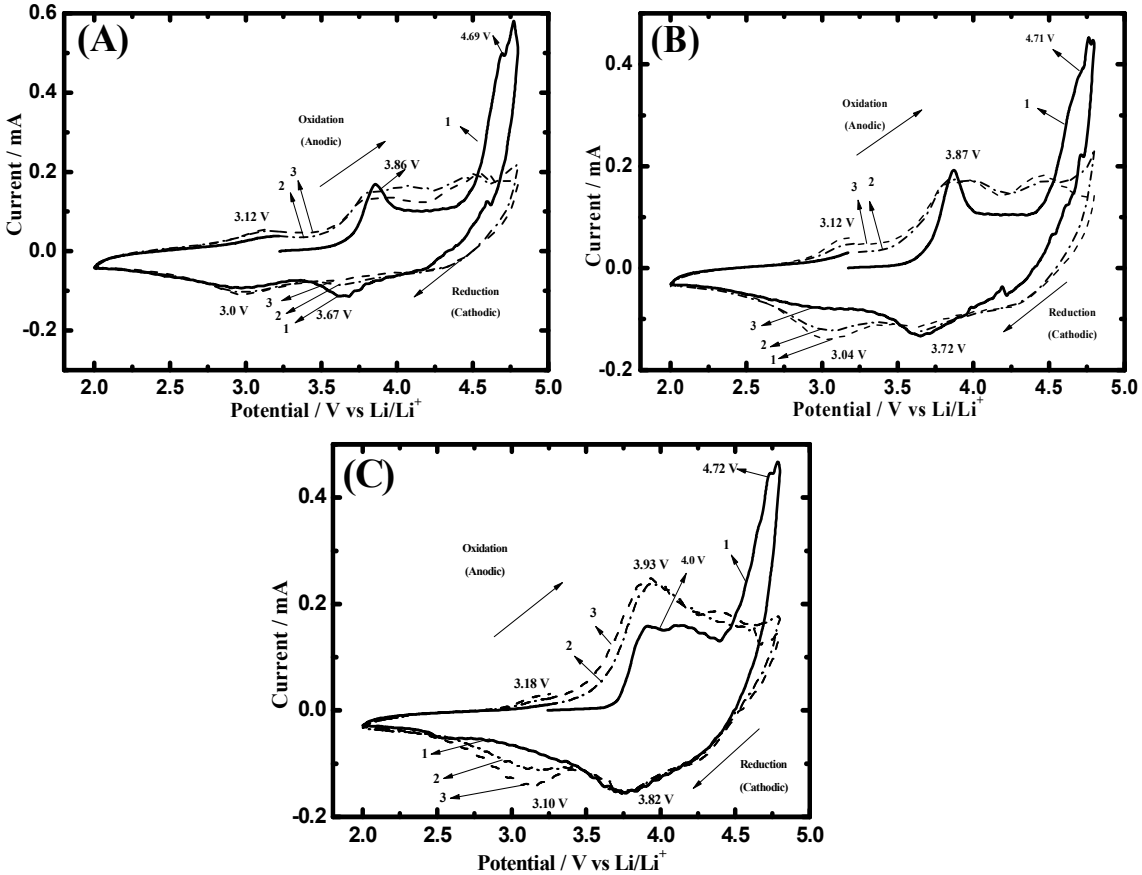

Fig. 6. Cyclic voltammograms of $0.5Li_2MnO_3$:$0.5LiMn_{0.5}Ni_{0.5}O_2$ sample S7 (A), S8 (B) and S9 (C) in a coin cell at a sweep rate of 0.1 mV s^{-1} for three consecutive cycles as indicated. Area of the electrode: 2.0 cm^2; and mass of the active material 3-5 mg.

New Journal of Chemistry Accepted Manuscript

In the first reverse sweep from 4.80 to 2.00 V, two cathodic current peaks are expected. In the first cyclic voltammogram of S7 sample (Fig. 6A), the cathodic current peak at 3.86 V corresponding to the reduction of Ni^{4+} appears clearly and reduction peaks of Mn^{4+} are noticed. This is supported by the fact that the capacity obtained corresponds to the $Ni^{+4/+2}$ and $Mn^{+4/+2}$ redox couple.[19] On repeatedly recording the voltammograms of sample S7 sample (Fig. 6A), the 4.60 V oxidation peak is absent from the second cycle onwards and the 3.86 V oxidation peak shifts in the negative direction to 3.79 V with low intensity. Furthermore, a new oxidation peak starts evolving at 3.12 V. In the reverse direction of the second cycle, the shallow 3.67 V starts decreasing and a new reduction current peak at 3.00 V starts evolving. The voltammogram of third cycle of samples S7 (Fig. 6A) confirms the features of the second cycle, and the 3.18 V oxidation peak as well as 3.00 V reduction peak become more intense. These voltammetric features of the S7 sample reveal the electrochemical activation of the lithium rich composite leading to an integrated electrode material.

The cyclic voltammograms of S8 sample recorded for three repeated cycles (Fig. 6B) reflect the features of S7 sample (Fig. 6A), but with a few minor changes observed. The 3.87 V oxidation peak appears clearer, and the 3.12 V oxidation peak as well as 3.04 V reduction peak become more intense in the second and third cycles (Fig. 6B) when compared with S7 sample (Fig. 6A). Thus, the cyclic voltammetric current features of S8 sample are more resolved than those of S7 sample. On the other hand, the cyclic voltammograms of S9 samples are superior to those of both S7 and S8 samples, in terms of sharpness of peaks as well as their reproducibility. The 3.10 V reduction peak formed in the second and third cycles are reproducible and well-resolved, in addition to the retention of 3.82 V for S9 sample (Fig. 6C), unlike the S7 sample with disappearance of 3.67 V in the third cycle and evolution of 3.00 V peak (Fig. 6A). The 4.00 V oxidation current peaks present in the second and third cycle voltammograms are well-formed. There are two pairs of redox peaks, namely,

New Journal of Chemistry Accepted Manuscript

3.18/3.10 V and 4.00/3.82 V current peaks, which originate from $Mn^{4+/3+}$ and $Ni^{4+/2+}$, respectively, redox reactions.[36] Thus, the voltammograms of S7, S8 and S9 samples suggest that the S9 sample is more electrochemically active and more reversible than the S7 and S8 samples. As expected, the charge-discharge cycling behaviour of S9 sample is superior to S7 and S8 samples, as discussed below.

3.7. Charge-discharge cycling: Galvanostatic charge-discharge curves of S5 - S9 samples for the first two cycles are presented in Fig. 7. All samples exhibit electrochemical activity when cycled between 4.80 and 2.00 V. During the first charging, two plateaus are observed, whereas appearance of voltage plateaus is not clear during the first discharge process. The differential plots (Fig. 7 insets) consist of peaks corresponding to both charge and discharge processes of the first cycle. The transition from the first charging plateau to the second plateau during the first cycle is 4.44 V for all samples. The values of capacity measured from the first plateau and the second plateau are listed in Table 3. In order to delineate the contribution of the two transition metal ions, the expected values of capacity are calculated from Ni and Mn on the basis of the composition $0.5Li_2MnO_3$:$0.5LiMn_{0.5}Ni_{0.5}O_2$. It is known that the oxidation states of Ni and Mn are +2 and +4, respectively, and therefore Ni and Mn only contribute for capacity in $LiMn_{0.5}Ni_{0.5}O_2$ part of the composite.[34, 35] Thus, the first plateau of the first charging process is attributed to the oxidation of Ni^{2+} to Ni^{4+}. The charging voltage plateau of this process merges with the activation of Li_2MnO_3 part of the composite at about 4.60 V. The combined processes of oxidation of Ni^{2+} to Ni^{4+} and reaction (1) provide charging capacity values of the second plateau as listed in Table 3. The first discharge curve exhibits a single plateau, as evidenced from the differential curves (Fig. 7 insets). In the second cycle, the charging potential curves are below those of the first cycle for all samples. Also, there is a single plateau, unlike two plateaus observed in the first charging curves. This is because Li_2MnO_3 part of the composite has become electrochemically active

New Journal of Chemistry Accepted Manuscript

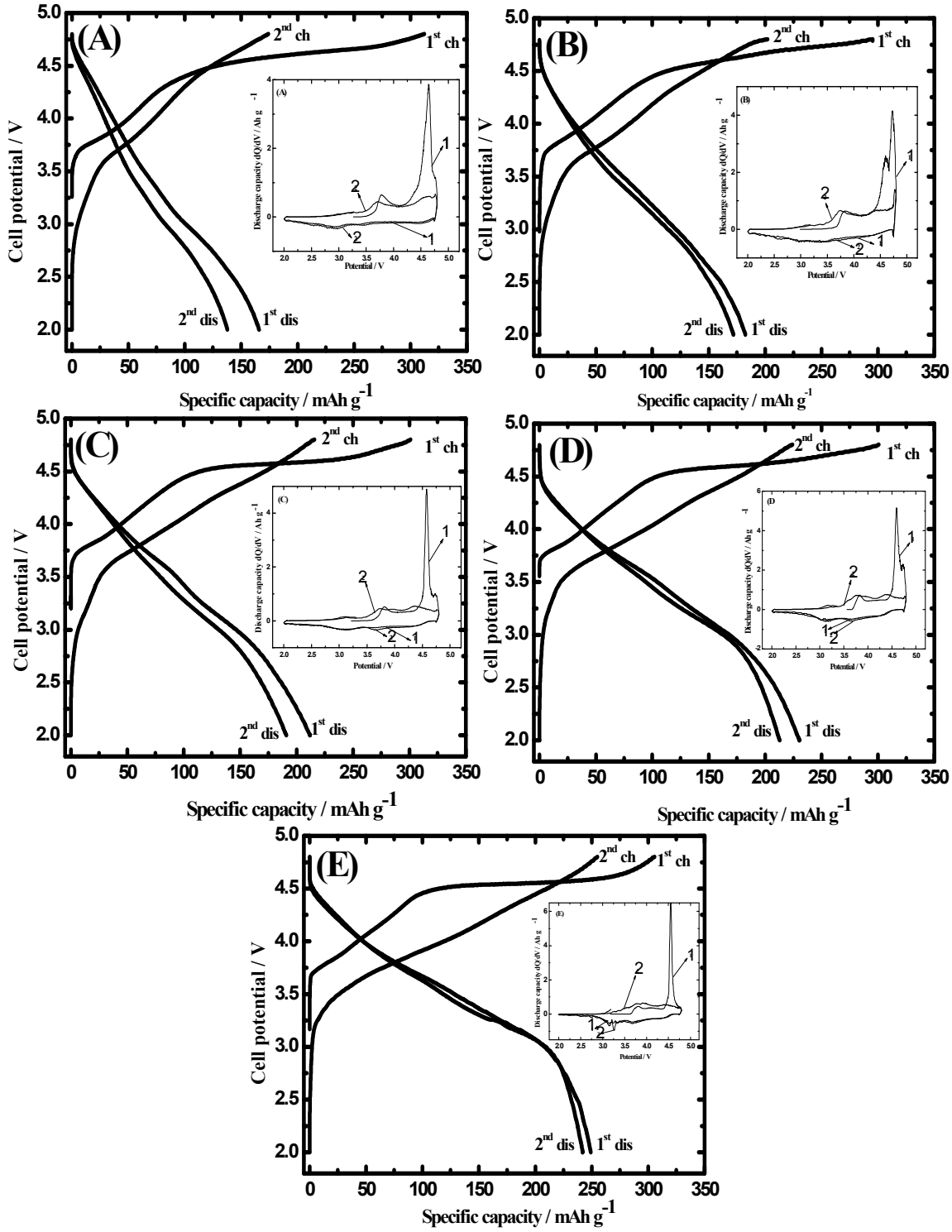

Fig. 7. Charge-discharge voltage profiles of $0.5Li_2MnO_3$:$0.5LiMn_{0.5}Ni_{0.5}O_2$ samples (A) S5, (B) S6, (C) S7, (D) S8 and (E) S9 in coin cells in the first and second cycle as indicated. Cell current: 100 μA; Electrode area: 2.0 cm^2 and mass of active material: 3-5 mg. Differential curves of the first and second cycle are shown as insets

New Journal of Chemistry Accepted Manuscript

during the first charge process, and subsequently integrated with $LiMn_{0.5}Ni_{0.5}O_2$ part. The integrated active material thus exhibits a single plateau in the second cycle. The discharge curves of the first and second cycle overlay with one another, thus indicating the compound is activated in the first charging step only. It is also seen that the coulombic efficiency of the first cycle is poorer than the second cycle, as detailed later. It is interesting to note that all samples (S5-S9) are electrochemically active with similar charge-discharge curves (Fig. 7). In the first cycle the charging capacity values up to 4.8 V are 312, 295, 301, 302 and 306 mAh g^{-1} respectively, for S5, S6, S7, S8 and S9 samples, whereas the corresponding values of discharge capacity are 166, 182, 220, 231 and 248 mAh g^{-1}. Thus there is a gradual increase in discharge capacity of the composite samples with an increase in preparation temperature. The coulombic efficiency of these samples in the first cycle, therefore, are 0.53, 0.62, 0.73, 0.77 and 0.81, respectively. The discharge capacity values obtained in the second cycle are 138, 172, 198, 213 and 242 mAh g^{-1} with coulombic efficiencies of 0.80, 0.85, 0.88, 0.95 and 0.96 for samples S5, S6, S7, S8 and S9, respectively. Thus there is a marginal decrease in discharge capacity, but improved efficiency in the second cycle in relation to the values obtained in the first cycle. The low efficiency of the first cycle is due to the irreversible reaction (reaction 1), which takes place during electrochemical activation of Li_2MnO_3.

The discharge capacity of a cathode material depends on several properties, which include morphology, particle size, surface area, porosity, crystalline nature, etc. It is expected that small particle size, large specific surface area, high pore volume and appropriate crystalline structure favour a high capacity. In the present study, the particle size increases, pore volume decreases and surface area decreases (Figs. 3 and 5) by increasing the preparation temperature. Thus, the trends of variation of these properties are expected to provide decreased capacity for samples from S5 to S9, in contrast to the obtained capacities (Fig. 7). It is therefore likely that the crystallinity of the composite samples influences more

New Journal of Chemistry Accepted Manuscript

than the rest of the properties, as the discharge capacity is found to increase with increased crystallinity of the samples (Fig. 2) in the present study.

Table 3. The first charging capacity values corresponding to the first plateau below 4.44 V and the second plateau between 4.44 and 4.80 V at a specific current of 25 mA g^{-1} for samples, irreversible capacity (IRC) loss and efficiency.

sample	First charge capacity (mAh g^{-1})			Discharge capacity (mAh g^{-1})	Coulombic efficiency (%)	IRC loss (mAh g^{-1})
	up to 4.4 V	between 4.4 and 4.8 V	Total capacity			
S5	109	203	312	166	53	146
S6	99	196	295	182	62	113
S7	101	200	301	220	73	81
S8	94	208	302	231	77	71
S9	98	208	306	248	81	58

The discharge capacity of 250 mAh g^{-1} obtained for S9 sample is comparable to the values reported in the literature for the $0.5Li_2MnO_3$:$0.5LiMn_{0.5}Ni_{0.5}O_2$.[34-36] Specific capacity values of 228 mAh g^{-1} for a sample prepared by self-combustion method,[35] 225 mAh g^{-1} for a sample prepared by co-precipitation method,[36] 234 mAh g^{-1} for a sample prepared by sol-gel route, 180 mAh g^{-1} for a sample prepared by self-directed chemical method[37] and 239 mAh g^{-1} for a sample prepared by self-template method[38] are reported. Thus, the integrated samples of $0.5Li_2MnO_3$:$0.5LiMn_{0.5}Ni_{0.5}O_2$ prepared in the present study deliver high discharge capacity.

3.8. Cycle-life test: Cycle-life data of the composite samples are shown in Fig. 8A. When cycled with cell current of 100 μA (Fig. 8A), the capacity values of S5, S6, and S7 decrease gradually from the initial values of 166, 18 and 223 mAh g^{-1} to 50, 80 and 95 mAh g^{-1}, respectively, at the end of 30 charge-discharge cycles. The capacities thus, decrease from their initial values by 30, 44 and 45 % mAh g^{-1} at the end of 30 charge-discharge cycles for

New Journal of Chemistry Accepted Manuscript

S5, S6 and S7 samples. Nevertheless, the capacity values of S8 and S9 samples are more stable than the S5 - S7 samples (Fig. 8A). The capacity decreases from 231 and 248 mAh g^{-1} in the first cycle to about 180 and 200 mAh g^{-1} in the second cycle for S8 and S9 samples, respectively. From the second cycle onwards, the discharge capacity is almost stable. The capacity values obtained for S8 and S9 samples in the 30th cycle, respectively, are 78 and 81 % of the values obtained in the first cycle. The stable discharge capacity of 210 mAh g^{-1} obtained for the composite samples prepared at 900 ^{o}C is considered as an extremely high value, which is attributed to the method of preparation adopted in the present study. For the purpose of cycling for larger number of cycles than shown in Fig. 8A, cells of S8 and S9 samples were cycled at 325 μA (100 mA g^{-1}) for 100 cycles (Fig. 8B). It is seen that a stable cycling behaviour is observed for both samples.

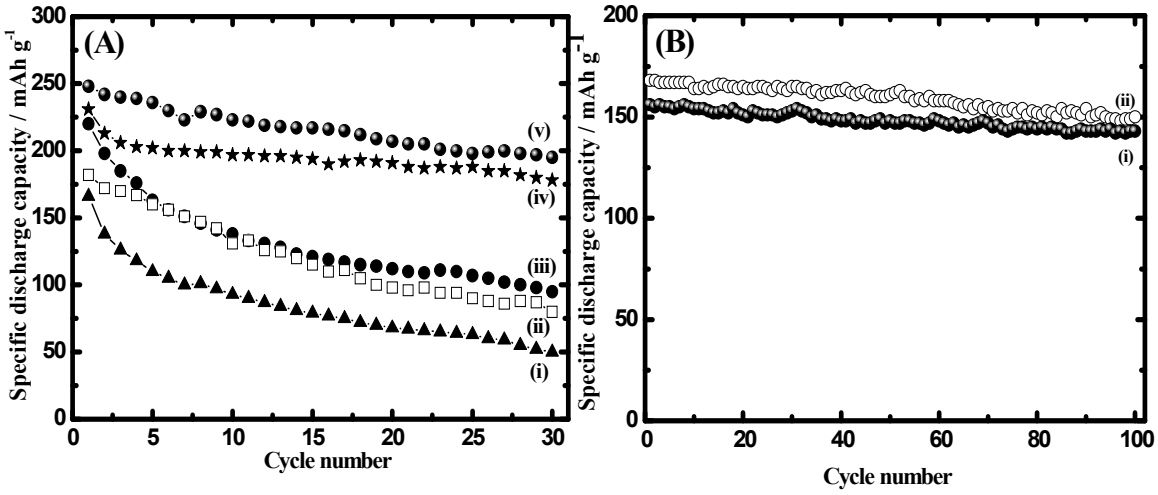

Fig. 8. Cycle life test of $0.5Li_2MnO_3$:$0.5LiMn_{0.5}Ni_{0.5}O_2$ samples S5 (i), S6 (ii), S7 (iii), S8 (iv) and S9 (v) at charge-discharge cell current of 100 μA and (B) S8 (i) and S9 (ii) at charge-discharge cell current of 325 μA. Electrode area: 2.0 cm^2; and mass of active material: 3-5 mg.

3.9. Rate capability: The rate capability of S7, S8 and S9 composite samples was studied by subjecting the cells to charge-discharge cycling at several specific currents at room temperature (Fig. 9). There is a decrease in discharge capacity of the three samples with an increase in current density, as expected. At all current densities, the capacity of S9 sample is

New Journal of Chemistry Accepted Manuscript

the highest and that of S7 sample is the least in agreement with the cyclic voltammetry (Fig. 6) and cycle-life test results (Fig. 8). About 100 mAh g^{-1} is obtained for S9 sample at a specific current of 500 mA g^{-1}. The high rate capability is attributed to porous nature of the materials.

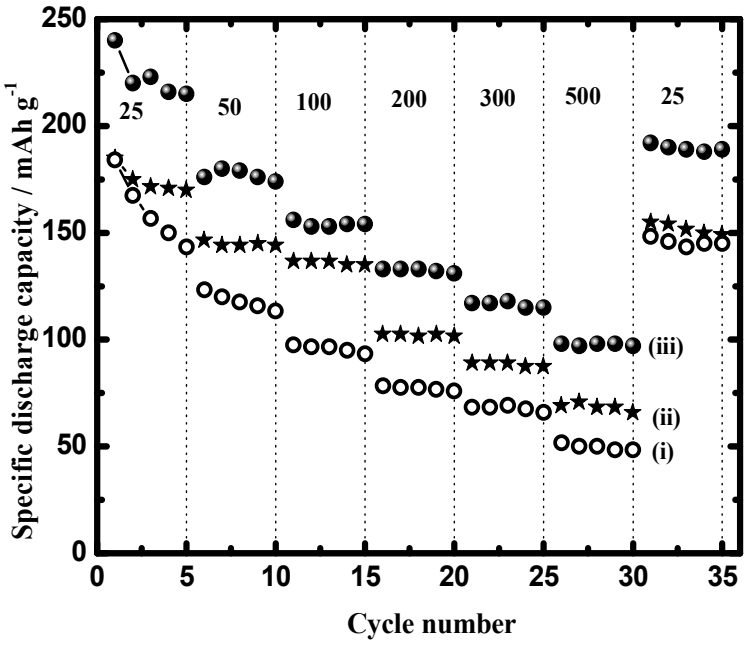

Fig. 9. Rate capability of $0.5Li_2MnO_3$:$0.5LiMn_{0.5}Ni_{0.5}O_2$ samples S7 (i), S8 (ii) and S9 (iii). Specific currents used for charge-discharge cycling of the coin cells are indicated in mA g^{-1}.

3.10. GITT technique: Galvanostatic intermittent titration technique (GITT) was employed to determine the diffusion coefficient of Li^+-ion (D_{Li+}).[39] Before GITT experiment, the electrode was activated by subjecting to one charge-discharge cycle in the voltage range between 2.00 and was started after 5 h of rest and its equilibrium potential (E_0) was reached. The electrode was subjected to delithiation by passing a constant charging current of 10 μA for a time τ so that the potential reached E_τ (Fig. 10A). Following the termination of charging current, the 4.80 V and disconnected from the circuit in discharged state at 2.00 V. The GITT experiment electrode was allowed to reach its new steady-state potential E_s, and the change in the steady-state potential $\Delta E_s = (E_s - E_0)$ was calculated. A plot of E versus t during charging

New Journal of Chemistry Accepted Manuscript

was linear (Fig. 10B). From the value of $\Delta E_\tau = (E_\tau - E_0)$ and ΔE_s, the diffusion coefficient D_{Li+} was calculated by using Eq. 2 [39].

$$D_{Li+} = (4/\pi\tau)\,(m_B V_m / M_B A)^2\,(\Delta E_s/\Delta E_\tau)^2 \qquad (2)$$

where m_B is the mass of the active material, M_B is the molar mass, V_m is molar volume and A is the area of the electrode. Typical experimental values were τ = 500 s, V_m = 29.05 cm^3 and m_B = 2.224 mg cm^{-2}. The values of D_{Li+} obtained for the sample S9 at potential 3.367 V is 1.61 x 10^{-10} cm^2 s^{-1}. The value of D_{Li+} is in good agreement with the reported values of Li-rich composites.[40-42]

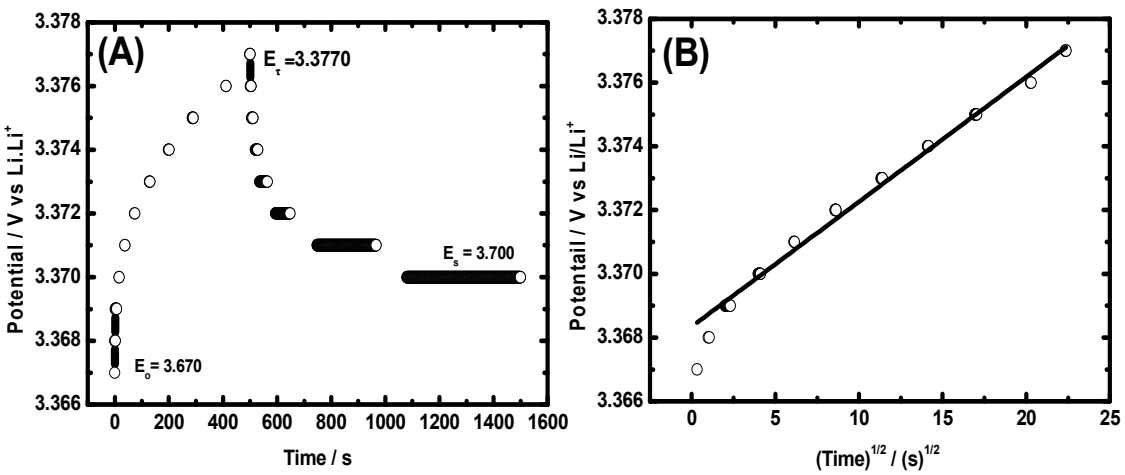

Fig.10. (A) Single titration at 3.261 V during Galvanostatic intermittent titration technique (GITT) curve of S9 sample, (B) Relationship of the cell voltage for the above titration and $t^{1/2}$.

4. Conclusions

Hierarchically porous layered composite samples of Li_2MnO_3 and $LiMn_{0.5}Ni_{0.5}O_2$ (composition: $Li_{1.2}Mn_{0.6}Ni_{0.2}O_2$) were prepared by reverse microemulsion method employing Pluronic acid (F068) as a soft template and studied as a positive electrode material. The product samples prepared at different temperatures possessed mesoporosity with broadly distributed pores at 3.6 nm and 30 nm. Pore volume and surface area decreased by increasing

New Journal of Chemistry Accepted Manuscript

the temperature of preparation. Nevertheless, the electrochemical activity of the composite was greater for the sample prepared at high temperature. The discharge capacity of the samples prepared at 800 and 900 ^{o}C was about 250 mAh g^{-1} at 25 mA g^{-1} with an excellent cycling stability. Both these composite samples exhibited high rate capability, but the 900 ^{o}C sample was superior to the 800 ^{o}C sample. A discharge capacity of 100 mAh g^{-1} was obtained at a specific current of 500 mA g^{-1}. The high rate capability was attributed to porous nature of the composite samples.

Acknowledgements: Authors thank Department of Science and Technology (DST), Government of India for funding under India-Israel project. TRP thanks University Grant Commission (UGC), Government of India for a senior research fellowship.

References

1. M. Winter and R. J. Broad, *Chem. Rev.,* 2004, **104**, 4245.

2. K. Matsuki and K. Ozawa, *Lithium Ion Batteries,* p.1, Wiley-VCH, Tokyo, 2009.

3. S. Wittingham, *Chem. Rev.,* 2004, **104,** 4271.

4. M .M. Thackeray, *Prog. Solid State Chem.,* 1997, **25,** 1.

5. M. H. Rossouw and M. M. Thackeray, *Mater. Res. Bull.,* 1991, **26,** 463.

6. P. Kalyani, S. Chitra, T. Mohan and S. Gopukumar, *J. Power Sources,* 1999, **80,** 103.

7. C. S. Johnson, S. D. Korte, J. T. Vaughey, M. M. Thackeray, T. E. Bobinger, Y. Shao Horn and S. A. Hackney, *J. Power Sources,* 1999, **81-82,** 491.

8. W. Tang, H. Kanoh, K. Ooi and Y. Wang, *J. Mater. Sci. Lett.,* 2000, **19,** 1361.

9. A. D. Robertson and P. G. Bruce, *Chem. Commun.,* 2002, **23,** 2790.

10. A. R. Armstrong and P. G. Bruce, *J. Power Sources,* 2005, **146,** 275.

11. D. Pasero, V. McLaren, S. DeSouza and A. R. West, *Chem. Mater.,* 2005, **17,** 345.

12. S- H. Park, Y. Sato, J-K. Kim and Y-S Lee, *Mater. Chem. Phys.,* 2007, **102,** 225.

New Journal of Chemistry Accepted Manuscript

13. D. Y. W. Yu, K. Yanagida, Y. Kato and H. Nakamura, *J. Electrochem. Soc.,* 2009, **156,** A417.

14. J. Lim, J. Moon, J. Gim, S. Kim, K. Kim, J. Song, J. Kang, W. B. Im and J. Kim, *J. Mater. Chem.,* 2012, **22,** 11772.

15. K. Numata, C. Sakaki and S. Yamanaka, *Solid State Ionics,* 1999, **117,** 257.

16. J. S. Kim, C. S. Johnson, J. T. Vaughey, M. M. Thackery, S. A Hackney, W. Yoon and C. P. Grey, *Chem. Mater.,* 2004, **16,** 1996.

17. S. H. Kang, P. Kempgens, S. Greenbaum, A. J. Kropf, K. Amine and M. M. Thackery, *J. Mater. Chem.,* 2007, **17,** 2069.

18. J. H. Lim, H. Bang, K. S. Lee, K. Amine and Y. K. Sun, *J. Power Sources,* 2009, **189,** 571.

19. F. Amalraj, D. Kovacheva, M. Talianker, L. Zeiri, J. Grinblat, N. Leifer, G. Goobes, B. Markovsky and D. Aurbach, *J. Electrochem. Soc.,* 2010, **157,** A1121.

20. X-Y. Yang, Y. Li, A. Lemaire, J-G. Yu and B-L Su, *Pure Appl. Chem.,* 2009, **81,** 2265.

21. M. Boutonnet, J. Kizling, P. Stenius and G. Mariey, *Colloids Surf.,* 1982, **5,** 205.

22. F. Kleitz, S. H. Choi and R. Ryoo, *Chem. Commun.,* 2003, **17,** 2136.

23. N. N. Sinha and N. Munichandraiah, *ACS Appl. Mater. Interfaces,* 2009, **1,** 1241.

24. N. N. Sinha, C. Shivakumara and N. Munichandraiah, *ACS Appl. Mater. Interfaces,* 2010, **2,** 2031.

25. N. N. Sinha and N. Munichandraiah, *J. Electrochem. Soc.,* 2010, **157,** A647.

26. P. Strobel and B. L. Andron, *J. Solid State Chem.,* 1988, **75,** 90.

27. C. H. Song, A. M. Stephan, S. K. Jeong, Y. J. Hwang, A. R. Kim and K. S. Nahm, *J. Electrochem. Soc.,* 2006, **153,** A390.

28. K. Karthikeyan, S. Amaresh, G. W. Lee, V. Aravindan, H. Kim, K.S. Kang, W.S. Kim, and Y. S. Lee, *Electrochem. Acta,* 2012, **196,** 3611.

New Journal of Chemistry Accepted Manuscript

29. Y. Ren, Z. Ma, R. E. Morris, Z. Liu, F. Jiao, S. Dai and P. G. Bruce, *Nat. Commun.,* 2013, **4,** 2015.

30. Y. Ren, F. Jiao and P. G. Bruce, *Microporous and Mesoporous Mater.,* 2009, **121,** 90.

31. K. M. Shaju, S. Rao and B. V. R. Chowdari, *Electrochim. Acta,* 2002, **48,** 145.

32. J. Reed and G. Ceder, *Electrochem. Solid-State Lett.,* 2002, **5,** A145.

33. S. H. Kang and M. M. Thackeray, *Electrochem. Commun.,* 2009, **11,** 748.

34. W. He, J. Qian, Y. Cao, X. Ai and H. Yang, *RSC Advances.,* 2012, **2,** 3423.

35. F. Amalraj, D. Kovacheva, M. Talianker, L. Zeiri, J. Grinblat, N. Leifer, G. Goobes, B. Markovsky and D. Aurbach, *J. Electrochem. Soc.,* 2010, **157,** A1120.

36. J. Wang, B. Qiu, H. Cao, Y. Xia and Z. Liu, *J. Power Sources,* 2012, **218,** 128.

37. O. Toprakci, H. A. K. Toprakci, Y. Li, L. Ji, L. Xue, H. Lee, S. Zhang and X. Zhang, *J. Power Source,* 2013, **241,** 522.

38. J. Liu, L. Chen, M. Hou, F. Wang, R. Che and Y. Xia, *J. Mater. Chem.,* 2012, **22,** 25380.

39. W. Weppner and R. A. Huggins, *J. Electrochem. Soc.,* 1977, **124,** 1569.

40. Z. Li, F. Du, X. Bie, D. Zhang, Y. Cai, X. Cui, C. Wang, G. Chen and Y. Wei, *J. Phys. Chem. C,* 2010, **114,** 22751.

41. H. Yu, Y. Wang, D. Asakura, E. Hosono, T. Zhang and H. Zhou, *RSC Adv.,* 2012, **2,** 8797.

42. Y. Bai, X. Wang, X. Zhang, H. Shu, X. Yang, B. Hu, Q. Wei, H. Wu and Y. Song, *Electrochim. Acta,* 2013, **109,** 355.

New Journal of Chemistry Accepted Manuscript

Graphical abstract

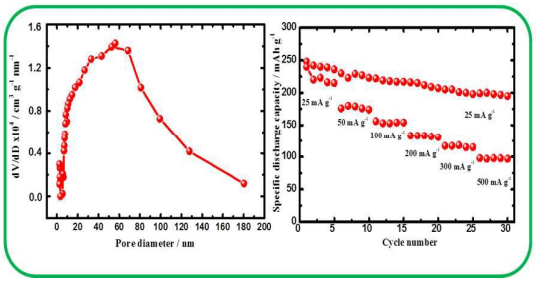

Highlight point:

"Lithium-rich manganese oxide with dual porosity as the cathode materials for the next generation high energy density Li-ion batteries".

New Journal of Chemistry Accepted Manuscript